

Mathematical modelling of polyamine metabolism in bloodstream-form *T. brucei*

Xu Gu¹, David Reid², Desmond J. Higham³ and David Gilbert⁴

¹MRC Human Genetics Unit, MRC Institute of Genetics and Molecular Medicine,

University of Edinburgh, Western General Hospital, Crewe Road, Edinburgh EH4 2XU, UK

²Gold Standard Simulations Ltd., The Rankine Building, Oakfield Avenue, Glasgow, G12 8LT

³Department of Mathematics and Statistics, University of Strathclyde, Glasgow, G1 1XH, UK

⁴School of Information Systems, Computing and Mathematics, Brunel University, Uxbridge, UB8 3PH, UK

Background: Trypanothione is critical for the vitality and virulence of *Trypanosoma brucei*, and sensitive to inhibition of the polyamine pathway.

Results: First mathematical model of polyamine biosynthesis in *T. brucei* is constructed and validated.

Conclusion: Interruption of polyamine synthesis via inhibition of multiple polyamine enzymes is optimal for treating *T. brucei*.

Significance: Model provides a useful framework for quantifying the reactions regulating trypanosomal growth.

1 Summary

In this paper, we present a first computational kinetic model of polyamine metabolism in bloodstream-form *Trypanosoma brucei*. The kinetic model is constructed based on information gleaned from the experimental biology literature and defined as a set of ordinary differential equations. We apply Michaelis-Menten kinetics featuring regulatory factors to describe enzymatic activities that are well defined. Uncharacterized enzyme kinetics are approximated and justified with available physical properties of the system. Optimization-based dynamic simulations were performed and inconsistent predictions prompted an iterative procedure of model refinement. General agreement between simulation results and measured data reported in various experimental conditions shows that the model has good applicability in spite of there being serious

gaps in the required data. Different chemotherapeutic strategies against *T. brucei* were investigated using this model and interruption of polyamine synthesis via joint inhibition of enzymes catalyzing reactions of de novo ornithine or AdoMet production together with other polyamine enzymes was identified as an optimal therapeutic strategy.

2 Introduction

The development of drugs to combat human African trypanosomiasis (HAT) has become a major public concern due to toxicity, inefficacy and availability problems with current drug treatments [1, 2]. Identification of potential drug targets within the *T. brucei* parasite is an invaluable tool for designing chemotherapeutic agents against the disease. A challenge in drug design arises from the similarity of metabolic pathways in parasitic protozoa and their mammalian hosts, resulting in toxicity to the host as well as the parasite. Anti-parasitic drugs that are efficient, non-toxic and affordable are urgently required.

Polyamines are ubiquitous cellular components that are essential for cell growth and division. Polyamine metabolism in mammalian cells has previously been studied using mathematical modelling [3]. Polyamine metabolism in *T. brucei* has a number of key features that distinguish it from polyamine metabolism in mammals. The major differences lie in the specificity of metabolites and enzymes as well as the associated regulation patterns. Most notably, the enzyme s-adenosylmethionine decarboxylase (AdoMetDC) is activated through dimerisation with an enzymatically inactive homologue termed prozyme. Moreover, spermidine (Spd), in addition to its plethora of other cellular roles, in trypanosomatids, is linked to two molecules of glutathione

to yield the redox active metabolite trypanothione, which is a compound critical for trypanosome viability and virulence.

Trypanosomes are sensitive to inhibition of the polyamine pathway. For example, it has been shown that trypanosomes depend on Spd for growth and survival, which ceases when Spd level drops below a certain threshold [4]. There is therefore considerable therapeutic potential in compounds that disrupt polyamine biosynthesis. The suicide inhibitor eflornithine (difluoromethylornithine, DFMO) kills trypanosomes by irreversibly interacting with ornithine decarboxylase (ODC) leading to reduced polyamine levels. Eflornithine is now the first line treatment used in HAT therapy. Inhibitors of AdoMetDC [5] have also been shown to be potently trypanocidal. These features have ensured that the polyamine pathway in *T. brucei* has been subject to investigation and details are available for enough of the enzymes to allow a mathematical model to be constructed and a recent attempt to model trypanothione metabolism in *Trypanosoma cruzi* (*T. cruzi*) also points to the value in modelling of this branch of metabolism in trypanosomatids.

Dynamic behaviour of complex biological systems is not deduced easily from collective descriptions of its individual parts; requiring instead a systematic approach with advanced computational technology. Mathematical modelling offers a route to achieve a system-level understanding [6, 7]. In the context of biological systems, mathematical models of metabolism allow improved understanding of the contribution of individual enzymes to the larger system. This can be achieved by studying the rates at which system components interact and physical laws that govern the reactions. Good models enable interpretation and predictions about the consequences of pathway perturbation that can supplement or even replace *in vivo* or *in vitro* experiments. Without a reliable model, it is difficult to understand how complexities evident from experimental data determine cellular behaviour.

In this paper, we develop a kinetic model of polyamine metabolism in blood-stream form *T. brucei*, derived from published information related to system components and their interactions. We are interested in seeking a model to reproduce what has already been observed and also to make predictions about the system to guide future experiments and guide drug design. Since mathematical models are manipulable, the mechanisms underlying the metabolic regulation of the polyamine biosynthesis can be evaluated *in silico*. This kinetic model aims at understanding the effectiveness of the anti-trypanosomal drug DFMO in detail and examining other polyamine enzymes as potential targets for anti-trypanosomal chemotherapy.

3 Materials and Methods

A detailed schematic representation of the trypanothione metabolic network is depicted in Fig. 1. This diagram indicates the complex interconnections between the main pathways, composed in parallel, which comprise the network. These are the polyamine biosynthetic pathway for the pro-

duction of Spd, the glutathione biosynthetic pathway for the production of glutathione and pentose phosphate pathway for production of the NADPH mediating the reduced trypanothione redox cycle from oxidized trypanothione disulfide. Spermine, which is a critical polyamine in mammalian cells, is not taken into account due to its negligible role in *T. brucei* [8, 9, 10, 11]. Here we study the contribution of the polyamine biosynthetic pathway to the regulation of total trypanothione contents (TSH_{tot} for short). Metabolites and enzymes constituting the polyamine pathway are highlighted in bold in Fig. 1. The following considerations were made to our model in order to study this pathway in isolation from the entire network.

Firstly, the involvement of the trans-methylation branch (responsible for the production of cystathionine via homocysteine) was limited to the first step describing the conversion of AdoMet into AdoHcy (S-adenosylhomo-cysteine). As observed in [12, 13], metabolic products of trans-methylation reactions (i.e homocysteine and cystathionine) are mostly secreted from trypanosomal cells, which leave their contributions in polyamine biosynthesis and regulation very minimal. AdoHcy, which is toxic if accumulated in cells [12], was also observed to remain unchanged under perturbed conditions in *T. brucei*, i.e. during 36 hours of DFMO treatment [13], and thus is treated as a constant metabolite in our study.

Secondly, we excluded glutathione biosynthesis and related reactions from consideration and modelled the biosynthesis of TSH_{tot} with a single-step reaction from Spd, catalyzed by a synthetic enzyme, named TSHSyn. In *T. brucei*, TSH_{tot} is synthesized in two steps. First, a single molecule of Spd is combined with glutathione to generate a glutathione-spermidine conjugate (GspdSH, not shown in Fig. 1). This is followed by the addition of a second Spd creating trypanothione from. It has been reported that both synthetase and amidase activity are associated with trypanothione biosynthesis in *T. brucei* [14] as well as in *Leishmania* parasites [15] and *Crithidia fasciculata* [16]. The conflicting activities of synthetase and amidase, which allow for a bidirectional response between the involved metabolites, may serve to modulate intracellular levels of the metabolites without additional protein synthesis or degradation of existing metabolites. There is however very limited information for enzyme kinetics of the intermediate steps of glutathione biosynthesis and the regulation mechanism between synthetase and amidase is not yet precisely characterized in *T. brucei*. This approximate description of TSH_{tot} biosynthesis reduces the degrees of freedom and diminishes the impact of unknowns in the model simulations. In the rate equation of TSHSyn, a regulatory term for the reaction product TSH_{tot} is explicitly included to reflect the self-regulation ability of involved metabolites i.e. Spd and TSH_{tot} , as if modulated by the amidase activity.

Thirdly, the link between TSH_{tot} and the remaining system (i.e. the pentose phosphate pathway in the grey box in Fig. 1) was modelled as a black box. Black-box modelling

is a popular approach for modelling chemical processes that lack physical insight or are highly abstract [17, 18]. This facilitates the practical construction of a useful model of polyamine metabolism with predictive capabilities; this can only be achieved when all intra-cellular metabolites are modelled as time-dependent variables. Black-box structures are parameterized descriptions, which can be approximated in the form of, for example, power series polynomials and fuzzy logic. In this study, a combination of a Hill equation and a linear decay function proportional to the concentration of TSH_{tot} is used to model this reaction (this is explained in detail in the next section). Inclusion of total trypanothione in the model allows us to quantify explicitly the consequences of polyamine interruption on cell growth arrest in the context of the model.

Finally, in *T. brucei* the lack of a classical arginase [19] has led to the identification of ornithine (Orn) uptake from blood as the main mechanism to accumulate this metabolite and the related kinetics were included in the model.

Model development involved converting the reaction scheme in Fig. 1 into a set of ordinary differential equations (ODEs). The ODE formalism has previously been employed to model quantitatively the glycolysis pathway in bloodstream-form *T. brucei* [20]. In our model the polyamine biosynthetic pathway is described mathematically by eight ODEs (Table 1), which associate the changes in concentration levels of system components (on the left) with the rate equations of enzymatic reactions involved (on the right). The ODE model takes exogenous methionine (Met_{exg}) and ornithine (Orn_{exg}) as the only inputs, since *T. brucei* does not have an efficient mechanism for the assimilation of exogenous putrescine (Put) and Spd, and relies on *de novo* synthesis to acquire these two polyamines [21, 22]. Concentrations of both external (Met_{exg} and Orn_{exg} in blood) and constant (AdoHcy) metabolites are fixed at their physiological levels.

In our study, simultaneous fitting against both the physiological steady state and *in vivo* DFMO-mediated polyamine inhibition reported in [10] is applied to tune the unknown parameters of the given model structure (refer to the section on Model Calibration for more details). DFMO-induced perturbation is the most comprehensive data source available for training the model (inhibition profiles being given for 6 out of 8 metabolites of the pathway in *T. brucei*); however, corrections had to be made before the dataset can be used (i.e. AdoMet dynamics, as explained later). Gene perturbation measurements on ODC [23], SpdS [21, 23], prozyme [24], AdoMetDC [25, 24] and TSHSyn [26], which are not used for training the model, are then employed as validation data to evaluate the candidate models.

It is important to point out that this modelling activity is not only challenged by the lack of prior knowledge, i.e. several kinetic parameters are absent, but also by the fact that experimental observations involve different trypanosome strains grown in different conditions - work by Fairlamb et al. was from trypanosomes grown in rats whilst

| Variables | Differential Equations |
|-----------------------|---|
| [Met] | $\frac{d[Met]}{dt} = V_{MetPt} - V_{MAT} + V_{MetRcy}$ |
| [AdoMet] | $\frac{d[AdoMet]}{dt} = V_{MAT} - V_{AdoMetDC^T} - V_{AHS}$ |
| [dAdoMet] | $\frac{d[dAdoMet]}{dt} = V_{AdoMetDC^T} - V_{SpdS}$ |
| [Orn] | $\frac{d[Orn]}{dt} = V_{OrnPt} - V_{ODC}$ |
| [Put] | $\frac{d[Put]}{dt} = V_{ODC} - V_{SpdS}$ |
| [MTA] | $\frac{d[MTA]}{dt} = V_{SpdS} - V_{MetRcy}$ |
| [Spd] | $\frac{d[Spd]}{dt} = V_{SpdS} - V_{TSHSyn}$ |
| [TSH _{tot}] | $\frac{d[TSH_{tot}]}{dt} = V_{TSHSyn} - V_{TSHCpt}$ |

Table 1: **The ODE model of polyamine metabolism.**

other gene-perturbation experiments involved in vitro cultivated strains. Inevitably, therefore, absolute quantification of metabolite levels which is strain and growth condition sensitive cannot emerge from such limited studies, although the general trends in quantification are conserved.

A cyclic workflow from model construction to model validation is often required to render models satisfactory. In the standard approach (see [27, 28] for details), and initial model topology is constructed that approximates the input-output relationship of the system is constructed, and then a parameter estimation process is applied to match a particular dataset against model structure. Once a candidate model is built in this way, it can be tested on validation data, i.e. data not used in the parameter estimation step. If the estimate-containing model demonstrates predictive power it may be considered to be relevant in describing the underlying processes. Where inconsistency emerges between model predictions and experimental observations the model is refined and iteratively evaluated against validation data.

Following the above system identification procedure, four candidate models were generated, which share the same topology but differ with respect to the mathematical representations of enzyme kinetics, as summarized in Table 2. The final model performed the best on both the estimation data and validation data and its description form the basis of the rest of this paper.

There are several instances where published observations conflict. For example, AdoMet levels in trypanosomes during ODC inhibition by DFMO treatment, were reported as being elevated 75 times by Fairlamb et al. [10] whilst levels of this metabolite were almost unchanged during DFMO treatment studied by Xiao et al. [23]. The parameter esti-

| No. | Descriptions | Results |
|---------------------|---|--|
| V1 | We modelled all enzymes on the basis of standard irreversible Michaelis-Menten (MM) kinetics and incorporated the regulatory effect of production inhibition where specified in the literature. | Model failed to fit Orn, Spd and TSH_{tot} dynamics (i.e. the trend of concentration changes). For example, within 12 hours of DFMO treatment, Orn linearly increased to almost 30 fold of the initial value, which was reported as having an exponential approach in the estimation data. Spd and TSH_{tot} were reduced by a small amount only, which disagrees with the considerable depletions reported in the literature. |
| V2 | We modelled the enzyme catalyzing Orn uptake (V_{upt}^{Orn}) with reversible MM kinetics, as we suspected that rate descriptions of Orn-centered reactions may be ill-characterized, but there is no available biological knowledge about <i>T. brucei</i> that can be used for postulating the rate equations. K_{eq} (equilibrium constant) and K_{mP}^{Orn} (Michaelis constant of product) associated with the reaction are estimated along with existing unknown parameters. | Orn dynamics under DFMO treatment were significantly improved in terms of the trend in transient concentration changes in comparisons to Model V1. No obvious improvements were seen for Spd and TSH_{tot} from the changes imposed on the rate expression of Orn uptake. The enzyme catalyzing the simplified reaction between Spd and TSH_{tot} may be ill characterized. |
| V3 | Since TSH_{tot} production from Spd is highly abstract in our system, selecting an appropriate function to approximate kinetics for TSHSyn is not straightforward. We refined enzyme kinetics catalyzing TSH_{tot} synthesis by adding a regulatory term representing product inhibition by TSH_{tot} to the irreversible MM kinetics used previously. This ensures resources not devoted to making TSH_{tot} when it is plentiful. | Simulation results agreed with the estimation data in terms of the trend in transient concentration changes for all metabolites under DFMO treatment. Together with the best set of parameter estimates, the model can also represent most of the validation data except SpdS-induced inhibition. A dramatic linear increase in Put is predicted in response to SpdS knockdown, which is counter to experimental observations that Put is not significantly accumulated. |
| V4 (final model) | On the basis of Model V3, we postulated an active regulation between SpdS on ODC through trial-and-error simulation experiments. This regulation prevents Put accumulation by restricting Put production rate when its consumption rate is largely reduced. | This model properly fits the DFMO-mediated profiles and reproduces all the validation data well, providing evidence of the validity of the model. This model is comprehensively explored in the rest of this paper. |

Table 2: **Different versions during the refinement of model design.**

mation process was applied to Model V4 to match the estimated data with an increased AdoMet concentration. Simulation results, however, predicted that AdoMet contents are largely unchanged and all other metabolites are well fitted. Thus, Xiao et al.'s observations on this metabolite were adopted for the parameter estimation data set together with observations made by Fairlamb et al. for all other metabolites.

Michaelis-Menten kinetics (for one substrate) were used to model the non-linear evolution of the enzymatic velocities of intra-cellular ODC, the MTA recycling enzyme (MetRcy) and the transporter of exogenous Met (MetPt). Michaelis-Menten kinetics with two substrates has been applied for the enzymes SpdS and MAT. More complex mechanisms have been employed for exogenous Orn uptake (OrnPt), AdoMetDC, TSHSyn and TSHCpt to which standard Michaelis-Menten kinetics are not appropriate (as analyzed below). Available parameter values for pathway enzymes are shown in Table 1 in the supplementary material. Regarding the information not available from the literature we made estimates by fitting the model to observed experimental data (in this case DFMO-mediated pathway profiles).

ODC catalyses the initial step in the pathway leading to Put production from Orn. ODC has an extremely short intra-cellular half-life in mammals, reportedly 15 min to 1 hr, which is in contrast to the more stable protein in *T. brucei*, which has a turnover rate greater than 6 hrs. A mathematical rate expression for ODC is modelled in the form below, which is subject to product inhibition by Put and postulated correlation of SpdS on ODC (see Table 2). When SpdS remains uninduced, parameter λ_{SpdS} is zero and thereby the catalytic capacity of ODC becomes time-independent. Under SpdS perturbations, a positive value has been deduced for parameter λ_{SpdS} from the given inhibitory profile of SpdS deactivation to mimic the temporal changes of SpdS activity over time and in this case the catalytic capacity of ODC becomes time-variant and influenced by the activity changes of SpdS.

$$V_{ODC} = V_{max}^{ODC} \cdot e(-\lambda_{SpdS} \cdot t) \cdot \frac{\frac{[Orn]}{K_{mOrn}^{ODC}}}{1 + \frac{[Orn]}{K_{mOrn}^{ODC}} + \frac{[Put]}{K_{iP}^{ODC}}} \quad (1)$$

AdoMetDC is responsible for the formation of dAdoMet, the aminopropyl donor for the biosynthesis of Spd from Put. As is the case for *T. brucei* ODC, *T. brucei* AdoMetDC is a stable enzyme and has a lower turnover rate than in mammalian cells. AdoMetDC is also a regulatory enzyme, regulated by an allosteric mechanism with 'prozyme', which is an enzymatically inactive close homologue of AdoMetDC itself. The regulation of AdoMetDC is induced by a conformational change of the prozyme structure, which alters the half-saturation constant of AdoMetDC activity. Willert et al. [29] discovered that in *T. brucei* neither AdoMetDC nor prozyme *per se* is sufficiently active to prompt normal

cell growth, and only the complex of AdoMetDC|prozyme can maintain the physiological level of Spd. Recent work by Willert and Phillips [24] has extended the subject to examining the influence of AdoMetDC RNAi inhibition and prozyme knockout on polyamine synthesis and parasite growth. A similar mechanism of allosteric regulation was also found for *T. cruzi* AdoMetDC [30].

The binding of AdoMetDC with prozyme contributes to dynamical control of metabolic fluxes in the polyamine pathway [29]. We represent the enzyme-ligand binding between AdoMetDC and prozyme as a one-step conformation system, with the plausible assumption that the ligand can interact rapidly with the enzyme as prozyme concentration is not comparable with AdoMetDC concentration [29], causing the reaction to occur at a rapid equilibrating rate following linear mass action kinetics (i.e. $[E] \gg [S]$). Because prozyme levels are restricted, AdoMetDC is present in trypanosomal cells in both ligand-occupied form and free form. Accordingly, we express the velocity equation of the total AdoMetDC as a superposition of two terms stemming from the individual forms of the enzyme (Eq. 2). The representation of regulatory capabilities in summation of distinct states has been verified for allosteric enzymes in [31].

$$V_{AdoMetDC^T} = V_{AdoMetDC^L} + V_{AdoMetDC^O} \quad (2)$$

where

$$\begin{aligned} V_{AdoMetDC^L} &= k_{cat}^{AdoPro} \cdot [AdoMetDC^T] \cdot (1 - \beta) \cdot \frac{\frac{[AdoMet]}{K_{mAdoMet}^{AdoPro}}}{1 + \frac{[AdoMet]}{K_{mAdoMet}^{AdoPro}}} \\ V_{AdoMetDC^O} &= \frac{k_{cat}^{AdoMetDC^O} \cdot [AdoMetDC^T] \cdot \beta \cdot \frac{K_{mAdoMetDC^O}^{AdoMet}}{K_{aPut}^{AdoMetDC^O}}}{1 + \frac{[AdoMet]}{K_{mAdoMet}^{AdoMetDC^O}} + \frac{[dAdoMet]}{K_{idAdoMet}^{AdoMetDC^O}} + \frac{[Put]}{K_{aPut}^{AdoMetDC^O}}} \end{aligned}$$

In these equations, $V_{AdoMetDC^L}$ and $V_{AdoMetDC^O}$ stand for the velocity contributed by the ligand-occupied (binding with prozyme) and free form of the enzyme, modelled as above. A factor β represents the percent of free-form AdoMetDC ($AdoMetDC^O$) taking up the total enzyme concentration ($[AdoMetDC^T]$), thus the ligand-occupied form ($AdoMetDC^L$) is expressed as $1 - \beta$ of the total concentration. Since the prozyme concentration is smaller than that of AdoMetDC [24], β is assumed to vary between 0.5 and 1 in order to reflect the experimental observation and still allow the ligand-occupied AdoMetDC to change within a physiologically feasible range. Note that in the above rate equations, Put and dAdoMet have a stimulatory and inhibitory effect respectively on the activity of free-form AdoMetDC but not on the AdoMetDC|prozyme heterodimer (the ligand-occupied form) [29]. We derived the activation constant $K_{aPut}^{AdoMetDC^O}$ from [32], which gave

a value of 1.5 μM . *T. brucei* AdoMetDC was thought to be insensitive to dAdoMet, which is in contrast to the strong product inhibition exerted by its counterpart in many other species (e.g. mammalian cells) [33]. A wide range of 1 to 1000 μM is applied for the parameter $K_{idAdoMet}^{AdoMetDC}$. The parameter estimates from *in silico* simulations can be used to qualitatively assess contradictory biological findings.

MAT catalyses production of AdoMet from Met in the presence of ATP. AdoMet plays an important role in a variety of cellular functions, such as methylation and sulphuration. Polyamines are not inhibitory to the enzyme within the range of 10 to 5000 μM , and positive cooperativity was only realised at higher concentrations of ATP with a Hill constant (n_{MAT}) equal to 2.0 [34]. The enzyme velocity is modelled in the form below, where AdoMet only exerts a weak inhibition on MAT, which is competitive with respect to the substrate Met.

$$V_{MAT} = V_{max}^{MAT} \cdot \left(\frac{\frac{[Met]}{K_{mMet}^{MAT}}}{1 + \frac{[Met]}{K_{mMet}^{MAT}} + \frac{[AdoMet]}{K_{iAdoMet}^{MAT}}} \right) \cdot \left(\frac{\left(\frac{[ATP]}{K_{mATP}^{MAT}} \right)^{n_{MAT}}}{1 + \left(\frac{[ATP]}{K_{mATP}^{MAT}} \right)^{n_{MAT}}} \right) \quad (3)$$

SpdS catalyses Spd biosynthesis from Put in the presence of dAdoMet, with methylthioadenosine (MTA) as a by-product. MTA is not detectable in mammals because of its rapid degradation rate [3, 35], which gives rise to the intra-cellular concentration of this compound being low [36]. Since no data is available for the physiological level of MTA in *T. brucei*, according to the observation in mammalian cells, MTA is assumed to hold a small value of 20 μM in our study. The kinetic mechanism of this enzyme is modelled below, subject to the product inhibition [37, 3]. Not that when SpdS remains wild-type, parameter λ_{SpdS} is 0, and thereby the catalytic capacity of SpdS becomes time-independent. Under perturbed conditions, the catalytic capacity of SpdS becomes time-variant and defined in accordance with the value of parameter λ_{SpdS} .

$$V_{SpdS} = V_{max}^{SpdS} \cdot e^{(-\lambda_{SpdS} \cdot t)} \cdot \frac{\frac{[Put]}{K_{mP}^{SpdS}}}{1 + \frac{[Put]}{K_{mP}^{SpdS}} + \frac{[Spd]}{K_{iD}^{SpdS}}} \cdot \frac{\frac{[dAdoMet]}{K_{mdAdoMet}^{SpdS}}}{1 + \frac{[dAdoMet]}{K_{mdAdoMet}^{SpdS}} + \frac{[MTA]}{K_{iMTA}^{SpdS}}}$$

MetRcy catalyses the synthetic transition from MTA to Met. MTA is recycled to Met via a series of en-

zymatic steps in trypanosomes [38]. It is first converted to methylthioribose-1-phosphate by MTA phosphorylase; the latter product is then metabolised to keto-methylthiobutyrate, and ultimately to Met [39]. Because of the importance of MTA recycling in cell viability, interference with Met metabolism has been explored as a potential drug target in mammals and *Plasmodium falciparum* [40, 41, 42]. In mammalian cells, Met can be regenerated via enzymatic catalysis of homocysteine [40]; however debate remains as to whether homocysteine remethylation exists in *T. brucei*, given that the enzyme catalysing this chemical transition is absent in other related parasitic species (e.g. *T. cruzi* and *Leishmania*) [43].

In our study, the MTA recycling path is considered as the unique source of Met reproduction, which is assumed to occur via a single-step reaction, as kinetics for the intermediate reactions are not known experimentally. In *T. brucei*, available quantitative descriptions for the recycling path are limited to the half-saturation constant of MTA phosphorylase with respect to its substrate MTA. Since the enzyme has a broad substrate specificity [44], the *in vivo* maximum velocity is hard to obtain, but it is assumed to hold a very high value [45]. Again, standard Michaelis-Menten kinetics are applied to describe the enzyme kinetics, shown below:

$$V_{MetRcy} = V_{max}^{MetRcy} \cdot \frac{\frac{[MTA]}{K_{mMTA}^{MetRcy}}}{1 + \frac{[MTA]}{K_{mMTA}^{MetRcy}}} \quad (5)$$

AHS catalyses the production of AdoHcy from AdoMet. The enzyme velocity is modelled as follows, subject to strong product inhibition by AdoHcy [46].

$$V_{AHS} = V_{max}^{AHS} \cdot \frac{\frac{[AdoMet]}{K_{mAdoMet}^{AHS}}}{1 + \frac{[AdoMet]}{K_{mAdoMet}^{AHS}} + \frac{[AdoHcy]}{K_{iAdoHcy}^{AHS}}} \quad (6)$$

AdoHcy is regarded as a constant metabolite during the *in silico* simulation and a methylation index of 2:1 [12] is assumed for the ratio of [AdoMet] to [AdoHcy] under wild-type conditions (resulting in the constraint [AdoHcy]=0.5·[AdoMet]) to approximate the relationship between the concentrations of the metabolites.

TSHSyn denotes the synthetic enzyme catalyzing one-step TSH_{tot} production from Spd in the model. Willert et al. [24] reported that in trypanosomes reduced trypanothione displays a sigmoidal response of the reaction rate to the concentration of intra-cellular Spd. We employed an irreversible Hill equation (with n_{Syn} standing for the Hill coefficient) to model this enzyme, which is characterized by competitive product inhibition by TSH_{tot} , shown as follows. This kinetic structure allows the model to mimic the *in vivo* state where TSH_{tot} levels can be compensated by elevating its production rate during *T. brucei* growth interruption (via reducing TSH_{tot} level).

$$V_{TSHSyn} = V_{max}^{TSHSyn} \cdot \frac{\left(\frac{[Spd]}{K_{mSpd}^{TSHSyn}}\right)^{nSyn}}{1 + \frac{[TSH_{tot}]}{K_{iTSH}^{TSHSyn}} + \left(\frac{[Spd]}{K_{mSpd}^{TSHSyn}}\right)^{nSyn}} \quad (7)$$

TSHCpt denotes the sink reaction responsible for TSH_{tot} involvement with the remaining system to prevent it from accumulated unrestrictedly. Designing a suitable expression for this abstract enzyme is challenging. A linear function of consumption rate (estimated with others) multiplying concentration of total trypanothione was initially proposed as a minimum consumption requirement; however the simulated behaviour of TSH_{tot} failed to reproduce either the steady-state or DFMO-perturbed data. We refined the rate definition by adding to this function an irreversible Hill equation representing enzyme-catalyzed breakdown of the metabolite. To relieve the pain due to the amount of existing unknowns, we approximated the consumption rate (in the liner function) as specific growth rate (μ) to which the consumption of total trypanothione is proportional in reality. This combined expression was later proved to be satisfactory for total trypanothione to be converged at the expected steady state and consumed rapidly under perturbation conditions.

The current representations for rate equations of TSHSyn and TSHCpt are capable of reproducing observed behaviour of trypanothione under various experimental conditions (see below). These kinetic structures will inevitably be different when the remaining metabolites in the network are integrated into this model.

$$V_{TSHCpt} = \mu \cdot [TSH_{tot}] - V_{max}^{TSHCpt} \cdot \frac{\left(\frac{[TSH_{tot}]}{K_{mTSH}^{TSHCpt}}\right)^{nCpt}}{1 + \left(\frac{[TSH_{tot}]}{K_{mTSH}^{TSHCpt}}\right)^{nCpt}} \quad (8)$$

MetPt is responsible for the uptake of exogenous Met in our model. Trypanosomes rely on a constant supply of Met, and *de novo* synthesis is energetically expensive [41, 47]. Again, standard Michaelis-Menten kinetics are applied to model MetPt as below

$$V_{MetPt} = V_{max}^{MetPt} \cdot \frac{\frac{[Met_{exg}]}{K_m^{MetPt}}}{1 + \frac{[Met_{exg}]}{K_m^{MetPt}}} \quad (9)$$

OrnPt is responsible for the uptake of exogenous Orn, which is modelled based on the reversible Michaelis-Menten kinetics. Exogenous Orn is considered as a constant supply into the system, with the plasma concentration assumed to

be 77 μM (representative in human serum [48]). Parameters K_{eq}^{Orn} and K_{mP}^{OrnPt} stand for the equilibrium constant and the half-saturation constant of product Orn, respectively.

$$V_{OrnPt} = ([Orn_{exg}] - \frac{[Orn]}{K_{eq}^{Orn}}) \cdot \frac{\frac{V_{max}^{OrnPt}}{K_m^{OrnPt}}}{1 + \frac{[Orn_{exg}]}{K_{mS}^{OrnPt}} + \frac{[Orn]}{K_{mP}^{OrnPt}}} \quad (10)$$

Overall, the ODE model of polyamine metabolism contains 40 kinetic parameters, where 20 are unknown and two are solved analytically. The incomplete model description makes parameter estimation a necessary step prior to dynamic simulations. In addition, to ensure unit consistency of the model parameters, we express all wild-type maximum velocities V_{max}^E (E refers to specific enzyme name) in units of μM per minute and hence in all these rate equations, the derivatives of the concentrations ($d[\text{Metabolite}]/dt$) are expressed in μM per minute. Some known enzyme velocities were measured in different units, i.e. μmol per minute per number of cells or per mg of protein, conversion of which into the desired units was required before carrying out model simulations. Unit conversions are elucidated in the methods section of the supplementary materials.

Model Calibration

Model calibration involves determination of model parameters that can reproduce the system behaviour. A common procedure is to first fit model parameters to experimental data generated by a reference cell type (wild type) and then test the estimates on data generated by a variation (mutant). In our study, we adopt a novel estimation methodology - the multi-objective optimisation algorithm MoPSwarm [49] - to estimate unknowns, where both the steady-state (wild type) and the perturbed (drug treated or genetic mutant) conditions of the pathway are handled simultaneously. It has been demonstrated in [49] that accounting for more than one state of the system in parameter estimation process is an advantageous approach for obtaining reliable parameter estimates. In this study, the model was trained via simultaneous fitting against both the physiological steady state and DFMO-mediated inhibition.

The polyamine model under steady-state (wild type) and DFMO-treated (perturbed) conditions differ in the mathematical representation of V_{ODC} , as enzyme activity of ODC (V_{ODC}) is a time-invariant parameter in the former case and a time-dependent exponential decay in the latter. Uptake kinetics of DFMO have not been measured. Despite the absence of a quantitative description, the DFMO-induced inhibition of ODC is well understood in a qualitative sense, where ODC activity decreased by more than 99% within 12-hour of treatment with DFMO [10]. ODC activity in response to DFMO is therefore modelled with an exponential decay function by multiplying the rate equation of ODC (defined in Eq. 1) with term $e^{-\lambda_{ODC} \cdot t}$ to reflect the time-dependent response of ODC activity to the drug inhibition,

shown below (Eq. 11). Parameter λ_{ODC} takes a value of 0.007 in this instance, solved by simple curve fitting using the qualitative description.

$$V_{ODC} = e^{(-\lambda_{ODC} \cdot t)} \cdot V_{max}^{ODC} \cdot e^{(-\lambda_{SpdS} \cdot t)} \cdot \frac{\frac{[Orn]}{K_{mOrn}^{ODC}}}{1 + \frac{[Orn]}{K_{mOrn}^{ODC}} + \frac{[Put]}{K_{iP}^{ODC}}} \quad (11)$$

Note that in this equation parameters λ_{ODC} and λ_{SpdS} correspond to different inhibitory scenarios, namely ODC inhibition (resulting from DFMO drug uptake or ODC enzyme perturbation) and SpdS inhibition, respectively. It is only when ODC and SpdS inhibition are applied in tandem that both parameters are given non-zero values. In other words, except in SpdS-inhibited conditions, λ_{SpdS} equals zero under both steady-state and DFMO-induced conditions as well as all other perturbed conditions.

Our choices of the initial metabolite concentrations are restricted to $\pm 20\%$ of the measured physiological levels when fitting the polyamine model to the given steady state. This helps the convergence of the algorithm from random positions in the search space. The solutions returned from the estimation procedure are ranked according to their importance in satisfying both pathway states using the root mean square of the two objectives with respect to an individual state, and the best trade-off solution with the highest rank is selected for investigation. More details are given in the supplementary materials (in the Results section) on the objective functions as well as the ranking method used for parameter estimation and selection.

Model metabolites simulated with the ‘best’ trade-off solution reached a steady state after less than the simulation time period of two days and maintained it until the end of day 6. The best trade-off set of parameter estimates is reported in Table 1 in the supplementary material. A good match between steady-state levels of polyamine metabolites from model predictions (termed the *basal* condition) and the reference data is shown in Table 3. We further investigated model sensitivity to different initial concentrations of pathway metabolites (varied by as much as $\pm 80\%$ of the estimated initial values). We found that the behaviour of these model variants converged to almost the same basal condition over a simulated time span of 4 days, indicating good stability. Simulation results for this are included in the supplementary material.

Model simulations of DMFO induction over an interval of 48 hours show good agreement with experimental data in terms of both exact values and transient changes in the metabolite concentrations, as shown in Fig. 2. A drastic decrease of Put was captured, which caused a significant increase in the dAdoMet level and a decrease in Spd. AdoMet was well fitted, and remained unchanged as observed in [23]. This may be attributed to the fact that free-form AdoMetDC is insensitive to the reaction product

dAdoMet as indicated by the high value of 970.6 μM predicted for $K_{idAdoMet}^{AdoMetDC}$ (inhibitory constant by dAdoMet), which agrees with the hypothesis made in [33]. An increase of Orn was observed within the first 12 hours of DFMO treatment, followed by attainment of an accurate steady state. Note that when plotting the time course of polyamines under perturbed conditions, the *basal* condition acts as the initial status for the simulation of DFMO-treated model, which also applies to model simulation under other perturbed conditions investigated below.

4 Results and Discussion

We set out to construct a model of polyamine metabolism in bloodstream form African trypanosomes given the potential of this pathway in providing therapeutic targets against the disease caused by trypanosomes. The task was constrained by a lack of many of the kinetic parameters required to produce a functioning kinetic model. A model of glutathione/trypanothione metabolism has recently been constructed for the related parasite, *T. cruzi*, and in that study it was decided to measure previously unknown parameters. Ultimately this is a productive route to generating model components. Here we take a different route, introducing two enzymatic reactions including the one-step conversion of Spd into TSH_{tot} catalyzed by TSHSyn and the consumption of TSH_{tot} for trypanosomal growth catalyzed by TSHCpt to link the polyamine pathway with total trypanothione without physically modelling glutathione and trypanothione metabolism and while still maintaining the predictive capability of the model. We ensured that the mathematical formulation of the rate equations approximated biochemical behaviour and applied the technique of parameter estimation to fill small gaps within the pathway where parameters are absent.

Comparison between model predictions using estimated parameter values and independent data sets obtained from distinct states of the system allows assessment of model use. To this end, data from available drug treatment and gene-knockdown perturbation experiments on ODC, SpdS, prozyme, AdoMetDC and TSHSyn are used as *validation data*. When simulating the model for each of the perturbation experiments, in the corresponding rate equations, an exponential decay function, in the form of $V_{max}^E \cdot e^{-\lambda_E \cdot t}$ with V_{max}^E representing the wild-type maximum velocity, is used to represent the inhibitory profile of the individual enzymes over time. Exponential decay constant, λ_E , was derived for individual instances by parameter fitting according to the given inhibitory profiles of corresponding enzymes. In each of the following perturbation experiments, all the kinetic parameters were fixed at the values reported in the supplementary materials, apart from those for the inhibited enzyme whose maximum velocity was decreased exponentially.

Model predictions on the consequences of ODC knockdown - DFMO is used to treat HAT and acts by inhibiting ODC

| | Met | AdoMet | dAdoMet | Orn | Put | MTA | Spd | TSH_{tot} |
|---|--------|--------|---------|------|-------|-----|------|-------------|
| from Model (μM) | 3341.5 | 20.3 | 8.2 | 86.2 | 587.3 | 20 | 2049 | 340 |
| from refs. (μM) [10] | 3978 | 19 | 9 | 43 | 517 | 20 | 2069 | 340 |

Table 3: **Basal condition of polyamine concentrations.**

with knock on effects on polyamine production, for example, reducing Put and Spd. As shown in Fig. 3, our model replicated the reduction in concentrations of Put, Spd and TSH_{tot} over 48 hours of model simulation where ODC activity is reduced by 90% within 24 hours of induction (as specified in Ref. [23]). dAdoMet serves to provide the aminopropyl group in Spd production which accumulates dramatically, while AdoMet is unchanged as reported in Ref. [23].

Model predictions on the consequences of SpdS knockdown - Spd plays multiple roles in trypanosomes including a critical role in producing the redox reactive thiol metabolite trypanothione, which underlines the sensitivity of trypanosomes to the loss of Spd through reduced capability to maintain cellular redox. SpdS has been validated as a potential drug target in *T. brucei* [21, 23]. Xiao et al. [23] observed that after 6 days of RNAi-mediated Spd depletion (SpdS activity knocked down by 90% within 2 days of induction), Spd and trypanothione decreased to 20% and 5% of the uninduced controls. Our model predicted a similar trend in concentration changes that Spd and TSH_{tot} reduced to 17% and 6% of the controls, as shown in Fig. 4(c) and 4(d). No significant changes were found for AdoMet and our model predicted this as well for this metabolite (see Fig. 4(a)).

Put is an interesting metabolite regarding its response to SpdS down-regulation. Xiao et al. reported a 45% decrease in Put concentration over 3 days after SpdS depression. Taylor et al. [21] also showed that, within 3 days, repressing SpdS by just 5% compared to wild type caused a 60% decline in Spd contents but, unexpectedly, no significant build up of Put was found. In *T. brucei* therefore, cellular overproduction of Put is avoided, possibly as excessive Put can elicit oxidative stress as reported in mammalian cells [50, 51].

In our model we included a term reflecting the apparently correlated regulation of SpdS on ODC activity (defined in Eq. 1) which serves to prevent Put accumulation, as demonstrated in Fig. 4(b). We observed that when this term is removed from the model while keeping the remaining parameters unchanged, a 90% knockdown of SpdS leads to a dramatic buildup in Put level (refer to the supplementary material for details). Inclusion of this regulatory term enables the model to simulate experimental observations. It will now be of interest to determine the biological basis of this regulation.

Model predictions on the consequences of AdoMetDC knockdown and prozyme knockout - AdoMetDC has already been validated as a drug target in *T. brucei*. Loss of

AdoMetDC or prozyme was observed to lead to decreases in Spd and trypanothione and to cell death [24]. In our model, simulations of prozyme knockout (over a simulated time span of 4 days with a complete removal of the ligand-binding form of AdoMetDC) and AdoMetDC knockdown (over a simulated time span of 6 days with a 70% down-regulation of total AdoMetDC concentration within 2 days of induction, as specified in Ref.[24]) both resulted in a large increase in Put levels and substantial reduction in Spd and TSH_{tot} . Simulation of the time-dependent effects on polyamine levels of Put, Spd and TSH_{tot} , induced by AdoMetDC knockdown and complete prozyme knockout are reported in Figs. 5(a) to 5(c). An 80% reduction due to prozyme knockout versus 65% reduction from AdoMetDC knockdown for Spd and a 94% reduction due to prozyme knockout versus 70% reduction from AdoMetDC knockdown for TSH_{tot} , were seen. These results are in good agreement with the tendencies described by real experimental observations [24].

We further compared the resulting TSH_{tot} content when the same degree of inhibition (70% knockdown applied to total AdoMetDC inhibition) was applied to ODC. Our model predicted a relatively lower TSH_{tot} level at the end of the simulated time span of 4 days from AdoMetDC inhibition (70% depletion) compared with that from ODC inhibition (40% depletion), which agrees with [25] that AdoMetDC could be a more promising chemotherapeutic target than ODC for *T. brucei*. Additionally, a 70% AdoMetDC knockdown or prozyme knockout caused an almost full depletion of dAdoMet accompanied by a 6-fold increase in Orn while AdoMet remained constant. These model predictions can be verified when the relevant experimental data is available. Our model simulations also reveal that activity of free-form (homodimeric) AdoMetDC ($V_{AdoMetDC^o}$) is 0.03% of the activity of heterodimer AdoMetDC|prozyme ($V_{AdoMetDC^L}$), which is consistent with the experimental observations [24] that the former is as low as <0.1% of the latter, indicating that prozyme reacting with AdoMetDC is a limiting factor for AdoMetDC activity.

Our model has also been validated on the consequences of inhibiting AdoMetDC activity by a specific inhibitor MDL73811 (5'-{[(Z)-4-amino-2-butenyl]methylamino}-5'-deoxyadenosine). When AdoMetDC was almost completely inhibited (to 2% of control enzyme activity within 1 hour of administration), a modest 33% decrease in Spd was observed by 4 hours post-administration of MDL73811 [25]. Our model predicted a similar 30% reduction in Spd over a simulated time span of 1 hour in response to the

strong AdoMetDC down-regulation (via reducing total AdoMetDC enzyme concentration $[AdoMetDC]^T$ to 2% of the control value) and a 20% depletion in TSH_{tot} was predicted. Simulation results are depicted in Fig. 5(d).

Model predictions on the consequences of TSHSyn knock-down - Trypanothione synthase (TryS), which catalyzes trypanothione production from Spd and glutathione has been recognised as a good drug target for trypanosomes [26]. It has been the focus of anti-trypanosomal research, owing not only to its significant role in trypanosomal viability but also its capability in regulating the levels of GspdSH, Spd and glutathione. In our model, this enzyme is represented as TSHSyn and a one-step production of total trypanothione from Spd is assumed (as stated previously in the methods section). Ariyanayagam et al. [26] reported that, within 3 days of TryS inhibition, TryS activity decreased 10-fold, giving rise to a 85% reduction in trypanothione level at the end of 8 days of RNAi induction, whereas the reactants of the reaction, Put and Spd, are not significantly increased. Despite the absence of glutathione in the model, knockdown simulations of TSHSyn (following the inhibitory profile of TryS) predicted a good match with the measured concentration changes of Put (no profound changes observed) and trypanothione (a 80% decrease in TSH_{tot} predicted) at the end of simulation duration of 8 days (illustrated in Fig. 6).

However, our model predicted a 10-fold increase in Spd level, which contradicts the measured dynamics. We postulate that this may result from the exclusion of glutathione in the model, which is found to accumulate markedly over 8 days of TryS inhibition in our simulation study. A potential elevation in Spd levels could be averted if it reacts with increased glutathione levels to produce TSH_{tot} . In the absence of quantitative inclusion of glutathione in our model, Spd was unconstrained to be rapidly increased. We tested this hypothesis by combining the 10-fold depletion of TSHSyn activity (at the end of 3 days) with an increased utilization of Spd (modelled through reduction in Spd production rate to 5% of the uncontrolled level at the end of 3 days). The model predicted a 30% drop in Spd accompanied with a considerable (90%) reduction in TSH_{tot} , supporting the possibility that Spd levels may be regulated by the interaction with glutathione. When adequate kinetic information becomes available regarding glutathione kinetics and intermediate metabolites in *T. brucei*, integration of the polyamine model with glutathione biosynthesis would be useful for improving quantitative predictions on inhibition consequences.

Sensitivity analysis - Sensitivity analysis describes changes of metabolite concentrations as result of changes in model parameters. We examined model sensitivity properties by running the model with the maximum velocity (V_{max}^E) of key pathway enzymes varied independently by $\pm 10\%$ of the nominal values. The model then evolves to a new steady state over a simulated time span of 6 days (plots not shown). Changes of maximum activities of enzyme MAT and MetPt resulted in a global effect on the sys-

tem, whereas some parameters influenced specific metabolites; for example, changes of TSHSyn led specifically to changes of Spd and TSH_{tot} and the function of TSHCpt is limited to TSH_{tot} only. The other input to the model, OrnPt, also showed an impact on Orn, Put and TSH_{tot} . With this analysis, we observed that when ODC is inhibited, Orn built up rapidly over 2 days leading to a new steady state, which is proportional to the degree of knockdown applied to ODC (illustrated in Fig. 7). This figure may explain why reversible inhibitors of ODC are not successful in killing trypanosomes as the extensive increase in Orn concentration (almost 7.5 times of the normal Orn value) will out-compete the reversible inhibitors interacting with ODC. The binding of the enzyme with irreversible inhibitors can however prevent competition from the substrate, but the inhibitors have to be sufficiently potent to cause apparent loss of TSH_{tot} content (discussed later).

We compared the changes in TSH_{tot} dynamics over a simulated time span of 5 days. Individual enzymes were subject to a 90% knockdown within 24 hours of simulation. These enzymes included ODC, SpdS, prozyme, MAT, OrnPt, MetPt and TSHSyn - enzymes involved in *de novo* synthesis of total trypanothione. Fig. 8(a) indicates that a 90% knockdown of each enzymes led to decreased TSH_{tot} , with levels dropping to less than 10% of the unperturbed level at the end of simulation span. MetPt, MAT, prozyme and OrnPt exhibit a much stronger inhibitory effect on TSH_{tot} than ODC and SpdS. TSHSyn displayed a faster converging trajectory after 48 hours of simulation and a more complete depletion of TSH_{tot} than all other enzymes.

We further analyzed TSH_{tot} concentration changes (at the end of a simulated time span of 5 days) with respect to different knockdown levels for individual enzymes. Fig. 8(b) revealed that all of these enzymes can almost completely deplete TSH_{tot} when they are each perturbed by at least 90%. This is recapitulated in Fig. 8(b), which indicates that when activity knockdown is more than 70%, TSHSyn has the strongest inhibitory effect on TSH_{tot} , whereas when the knockdown is less than 70%, MAT, MetPt, Prozyme and OrnPt exert the most effective control on TSH_{tot} reduction. Under all scenarios, ODC and SpdS displayed a relatively weaker inhibitory impact on TSH_{tot} . We observed that a 70% loss of ODC and SpdS led to the same effect as a 60% loss of TSHSyn or a 50% reduction of MAT, MetPt, Prozyme or OrnPt, indicating that to achieve the same level of TSH_{tot} depletion (70%), the knockdown strength required for different enzymes should follow $ODC, SpdS > TSHSyn > MAT, MetPt, Prozyme, OrnPt$. This could point to the enzymes MAT, MetPt, Prozyme and OrnPt as good potential drug targets, which lead to TSH_{tot} depletion with only small perturbations.

Combination chemotherapy for T. brucei. Enzymes responsible for polyamine biosynthesis are proven drug targets. Simulations generated by our model indicate that strong down-regulation of polyamine pathway enzymes including ODC, prozyme, SpdS and TSHSyn lead to reduc-

tions in TSH_{tot} levels, demonstrated to be potential targets for drug design.

The use of mathematical models not only provides a mechanistic understanding but can also drive new and more effective experiments. Combination chemotherapy for African sleeping sickness is attractive as it offers the potential for lower doses of drugs and reduced risk of resistance emerging for individual compounds. We are particularly interested in enzyme(s) that, when used in tandem with weak perturbation of other enzymes, result in a similar or even more potent inhibitory effect than when these enzymes alone are strongly perturbed.

Studying effects of inhibiting pairs of enzymes on TSH_{tot} , as illustrated in Fig. 9(a), shows that a combination of a 70% knockdown of enzyme MAT, prozyme or OrnPt with a weak (10%) down-regulation of ODC produces a similar effect on TSH_{tot} depletion as when ODC is almost completely removed. In conjunction with a 50% loss of MAT, prozyme or OrnPt, a weaker TSH_{tot} inhibition is obtained at the end of a simulated time span, but a faster depletion rate is displayed over the first 24 hours of inhibition than using a 90% ODC knockdown alone. A 10% prozyme depression (Fig. 9(b)), together with a 50% down-regulation of MAT or OrnPt reduced TSH_{tot} concentration to the same level at the end of a simulated time span as when only a 50% prozyme depression was applied. In conjunction with a 70% MAT or OrnPt down-regulation, the same 10% prozyme knockdown reduced TSH_{tot} to the same extent as a 90% prozyme knockdown alone. Furthermore, combining the same 10% prozyme knockdown with a 70% loss of ODC resulted in the same degree of TSH_{tot} depletion as lower-level joint perturbations (50%) with MAT or OrnPt.

In individual cases, combining a 10% knockdown of ODC or prozyme with a 70% TSHSyn inhibition reduced TSH_{tot} to the same amount as when the respective enzyme is perturbed by 90%, but with a slower inhibitory trajectory compared to combination therapies with MAT and OrnPt. When prozyme is reduced by less than 30%, all other enzymes have to be down-regulated by at least 90% in order to obtain the same level of TSH_{tot} depletion as a 90% prozyme depression alone (results not shown).

Fig. 9(c) to 9(d) support our previous conclusion that TSHSyn and prozyme alone are capable of adequately removing TSH_{tot} when it is subject to a sufficiently strong deactivation. As indicated in Fig. 9(c), the combination of a down-regulation of 70% in prozyme with a 70% depression of enzyme MAT produces the same temporal dynamics and final depletion of TSH_{tot} as a 90% prozyme knockdown alone. The maximum level of TSH_{tot} depletion occurs when prozyme (knocked down by 50% or 70%) is combined with a more potent 90% MAT down-regulation. Combining a 70% loss of prozyme with a medium to strong OrnPt perturbation can lead to a similar level of TSH_{tot} depletion, but not as strong as exerted by MAT. In Fig. 9(d), when TSHSyn is down-regulated by more than 50%, down-regulation of MAT or OrnPt by as much as 70% is required in tandem to ob-

tain the same level of TSH_{tot} depletion as a 90% TSHSyn down-regulation alone. We observed that even though combination therapies for TSHSyn and prozyme result in approximately the same level of TSH_{tot} depletion at the end of the simulated time span, they exhibited faster inhibitory trajectories, giving rise to more TSH_{tot} removal at earlier stages (the first 2-3 days of simulation span, see Fig. 9(d)). In both cases, combining a 70% knockdown of prozyme or TSHSyn with a 70% OrnPt down-regulation led to the same final TSH_{tot} level, but with slower temporal dynamics than other strategies over the same duration.

As indicated in Fig. 8, MAT and MetPt knockdown both result in almost the same depletion pattern for TSH_{tot} . As such, MetPt related perturbation was found to be applicable to the perturbation experiments carried out here in the same way as MAT. It has been verified that a constant supply of Met is imperative for trypanosomal cell growth [41, 47], supporting the credibility of the predictions made by this model. Similarly, the results observed for ODC are applicable to SpdS, however SpdS displayed a better inhibitory effect than ODC (likely due to the regulatory link predicted for the enzymes) but still not comparable with that from MAT or OrnPt.

The combination chemotherapeutic strategy suggests that enzymatic reactions of AdoMet production and Orn uptake, catalyzed by MAT and OrnPt, respectively, are key regulatory points in the pathway. When used alone or in tandem with weak down-regulation (i.e. 10%) of other enzymes, a moderate perturbation (i.e. 50%) of MAT and OrnPt exhibited a strong inhibitory impact on the total trypanothione production, with the former being more effective than the latter, in particular, when MAT knockdown is used in conjunction with medium or strong perturbation of prozyme and TSHSyn. The regulation of polyamine synthesis via MAT or OrnPt is likely to be a good chemotherapeutic target.

Conclusions - Mathematical models of metabolism have begun to find utility in drug discovery. One of the most useful and advanced models is that of glycolysis in protozoan *T. brucei*, the causative agent of HAT. Here we present a first model of a second branch of metabolism, the polyamine pathway, which can be linked to glycolysis via the second route of glucose metabolism in *T. brucei*, the pentose phosphate pathway that creates NADPH, which is the ultimate source of electrons required in reduction of trypanothione and the cell's primary reactive thiol species.

This model complements a recent attempt at modelling trypanothione metabolism in the related parasite *T. cruzi* [52]. The *T. cruzi* model focuses on the glutathione synthesis branch and the redox cycle of trypanothione. Polyamine synthesis, which is the focus of this work, is not included. Our simulation results (Fig. 8) agreed with observations made in the *T. cruzi* model that at 80%-100% down-regulation, most of the involved enzymes were found to be essential for parasite survival. In particular, TSHSyn (TryS in the *T. cruzi* model) has to be inhibited by 70% to suffi-

ciently deplete trypanothione contents, which is consistent between the two models. Both studies attempt to identify promising therapeutic strategies and this issue is viewed from the aspect that "suitable drug targets should be enzymes for which low pharmacological inhibition have a high impact on pathway function [52]". Pathway enzymes in the *T. cruzi* model were ranked according to control efficiency of individual enzyme and simultaneous inhibition of those enzymes with top scores were recommended as being good candidates for multi-target strategies, whereas in our *T. brucei* model, different combination therapies of key pathway enzymes were simulated and time-dependent concentration changes were measured against total trypanothione contents (Fig. 9(a) to 9(d)), providing us with a direct comparison among alternatives. We would like to take this work further by merging these two models to evaluate the perturbation effect on trypanothione level when the good targets identified from the respective work are jointly used. However, this is challenged considerably not only by the differences in the specificity of parameter values but also the kinetic reactions specific to individual organisms. For example, the cysteine uptake reaction that was not modelled in the *T. cruzi* model has proven to be critical for trypanosomal survival in *T. brucei* [47]. Additionally, both organisms can synthesize Spd de novo from dAdoMet and Orn but *T. cruzi* also holds the capability to assimilate exogenous Spd (only this uptake reaction was modelled in the *T. cruzi* model). Integration of these models could further assist in gaining an in-depth understanding of the overall metabolic system in trypanosomes.

Our modelling activities focused on studying the effectiveness of DFMO the first line drug licensed to target stage 2 HAT. Previous work has generated a significant amount of information regarding the network topology and kinetic analysis of many of the enzymatic reactions has made kinetic modelling possible. However, parameters for a significant number of the enzymes involved in the pathway were unknown. Therefore it was necessary to introduce assumptions and simplifications to the pathway were required. Qualitative knowledge of the pathway guided the assumptions made and optimization-enabled dynamic simulations were used to test how assumption-containing models performed relative to outputs measured in experiments. Discrepancies between model simulations and experimental observations prompted a cyclic procedure of model design. All proposed models share the same pathway topology but differ in mathematical expressions of the enzyme rate equations. We demonstrated that one model (V4 in Table 2) faithfully reproduces most experimentally measured properties of the pathway. The model can be further tested as new information becomes available from experiments aimed to measure fluxes through the pathway, as proposed in the silicon trypanosome project [53].

The model already offers opportunities to explore new strategies for targeting this pathway in anti-trypanosomal drug design. Combination chemotherapeutic studies

revealed that most polyamine enzymes can influence polyamine biosynthesis, but when targeted alone, high levels of inhibition are required to inhibit the pathway sufficiently to kill cells. Most importantly, reactions catalyzed by enzyme MAT or OrnPt appear to be critical control points of the pathway, with MAT being preferable than OrnPt. Moderate disruption of MAT or OrnPt, both in isolated and joint form, led to dramatic changes in polyamine concentrations as well as total trypanothione contents. Our study also shows that prozyme and TSHSyn could be used for multi-target therapy but only when they are potentially inhibited (at least 50% knockdown) together with similar down-regulation of MAT or OrnPt. Combined down-regulation of key pathway enzymes offers an effective chemotherapeutic strategy. The additional requirements for regulatory approval of combination therapies makes de novo production of combination therapies difficult, but it is worth noting that for HAT it was possible to introduce a nifurtimox-eflornithine combination therapy (NECT) which has advantages over eflornithine monotherapy alone. Metabolomics analysis did not indicate a role in polyamine pathway inhibition by nifurtimox [19], however the precedent to introduce, rapidly, a combination partner to work alongside eflornithine has been set.

In conclusion, it has been necessary to include multiple assumptions and simplifications to build a model of polyamine metabolism in *T. brucei* because insufficient data was available to produce a full description. Notwithstanding, the available of several datasets where measurements of metabolite levels following pathway perturbation has enabled us to adjust assumed parameters and simplifications in a way that allows reasonable simulations of measured activity. The model has then been used to make predictions on potential co-inhibition of different enzymes of the pathway to inform possible strategies for combination chemotherapy and can report on possible regulatory components of the pathway which can now be approached experimentally. The basic model description here can be further improved as new information becomes available in *T. brucei* on specific kinetic parameters of enzymes in the pathway and measured metabolite levels under different perturbed conditions.

Acknowledgement

XG is grateful to Professor Ray Welland (University of Glasgow, UK) for financial support during her PhD when this work was initiated. The authors thank to Professor Michael P. Barrett (Glasgow Biomedical Research Centre, University of Glasgow) for his considerable and invaluable contributions to the biological aspect of the paper. The authors are indebted to Associate Professor Barbara M. Bakker (University of Groningen, The Netherlands) and Dr. Jurgen Haanstra (University of Groningen, The Netherlands) for proof reading and useful discussions.

References

- [1] Sylke Muller, Eva Liebau, Rolf D. Walter, and R. Luise Krauth-Siegel. Thiol-based redox metabolism of protozoan parasites. *Trends in Parasitology*, 19(7):320–327, 2003.
- [2] Julio F. Turrens. Oxidative stress and antioxidant defense: a target for the treatment of diseases caused by parasitic protozoa. *Molecular Aspects of Medicine*, 25:211–220, 2004.
- [3] Carlos Rodriguez-Caso, Raul Montanez, Marta Cascante, Francisca Sanchez-Jimenez, and Miguel A. Medina. Mathematical modelling of polyamine metabolism in mammals. *The Journal of Biological Chemistry*, 281(31):21799–21812, 2006.
- [4] O. Heby, L. Persson, and M. Rentala. Targeting the polyamine biosynthetic enzymes: a promising approach to therapy of african sleeping sickness, chagas’ disease and leishmaniasis. *Amino Acids*, 33:359–366, 2007.
- [5] Cyrus J. Bacchi, Reto Burn, Simon L. Croft, Karen Allicea, and Yvonne Buhler. In vivo trypanocidal activities of new s-adenosylmethionine decarboxylase inhibitors. *Antimicrobial Agents and Chemotherapy*, 40(6):1448–1453, 1996.
- [6] Eberhard O. Voit. *Computational Analysis of Biochemical Systems: A Practical Guide for Biochemists and Molecular Biologists*. Cambridge University Press, 2000.
- [7] Hiroaki Kitano. Systems biology: a brief overview. *Science*, 295(5560):1662–1664, 2002.
- [8] Mark R. Ariyanayagam and Alan H. Fairlamb. Ovothioli and trypanothione as antioxidants in trypanosomatids. *Molecular & Biochemical Parasitology*, 115:189–198, 2001.
- [9] Vivian Bellofatto, Alan H. Fairlamb, Graeme B. Henderson, and George A. M. Cross. Biochemical changes associated with α -difluoromethylornithine uptake and resistance in *trypanosoma brucei*. *Molecular and Biochemical Parasitology*, 25:227–238, 1987.
- [10] Alan H. Fairlamb, Graeme B. Henderson, Cyrus J. Bacchi, and Anthony Cerami. In vivo effects of difluoromethylornithine on trypanothione and polyamine levels in bloodstream forms of *Trypanosoma brucei*. *Molecular and Biochemical Parasitology*, 24:185–191, 1987.
- [11] K. Kaur, K. Emmett, P. P. McCann, A. Sjoerdsma, and B. Ullman. Effects of DL- α -difluoromethylornithine on *leishmania donovani* promastigotes. *J. Protozool*, 33:518–521, 1986.
- [12] Cyrus J. Bacchi, Burt Goldberg, Joanne Garofalo-Hannan, Donna Rattendi, Peter Lyte, and Nigel Yarlett. Fate of soluble methionine in African trypanosomes: effects of metabolic inhibitors. *Biochemistry*, 309:737–743, 1995.
- [13] Nigel Yarlett and Cyrus J. Bacchi. Effect of dl- α -difluoromethylornithine on methionine cycle intermediates in *trypanosoma brucei brucei*. *Molecular and Biochemical Parasitology*, 27:1–10, 1988.
- [14] Sandra L. Oza, Mark R. Ariyanayagam, Niall Aitchison, and Alan H. Fairlamb. Properties of trypanothione synthetase from *trypanosoma brucei*. *Molecular & Biochemical Parasitology*, 131:25–33, 2003.
- [15] Paul K. Fyfe, Sandra L. Oza, Alan H. Fairlamb, and William N. Hunter. *Leishmania* trypanothione synthetase-amidase structure reveals a basis for regulation of conflicting synthetic and hydrolytic activities. *Journal of Biological Chemistry*, 283:17672–17680, 2008.
- [16] Sandra L. Oza, Mark R. Ariyanayagam, and Alan H. Fairlamb. Characterization of recombinant glutathionylspermidine synthetase/amidase from *crithidia fasciculata*. *Journal of Biochemistry*, 364:679–686, 2002.
- [17] Eduardo D. Sontag. Some remarks on input choices for biochemical systems. *Optimization and Control (math.OC)*, 2006. Available at <http://arxiv.org/abs/math/0606261v1>.
- [18] Lennart Ljung. Some aspects on nonlinear black-box modeling in system identification. Technical report, Linköpings Universitet, 2007.
- [19] Isabel M. Vincent, Darren J. Creek, Karl Burgess, Debra J. Woods, Richard J. S. Burchmore, and Michael P. Barrett. Untargeted metabolomics reveals a lack of synergy between nifurtimox and eflornithine against *Trypanosoma brucei*. *PLoS Negl Trop Dis.*, 6(5), 2012.
- [20] Barbara M. Bakker. *Control and regulation of glycolysis in Trypanosoma brucei*. PhD thesis, Vrije Universiteit, 1998.
- [21] Martin C. Taylor, Harparkash Kaur, Bernard Blessington, John M. Kelly, and Shane R. Wilkinson. Validation of spermidine synthase as a drug target in african trypanosomes. *Biochem. J.*, 409:563–569, 2008.
- [22] C. J. Bacchi, H. C. Nathan, S. H. Hutner, P. P. McCann, and A. Sjoerdsma. Polyamine metabolism: A potential therapeutic target in Trypanosomes. *Science*, 210:332–334, 1980.
- [23] Yanjing Xiao, Diane E. McCloskey, and Margaret A. Phillips. Rna inference-mediated silencing of ornithine

- decarboxylase and spermidine synthase genes in *Trypanosoma brucei* provides insight into regulation of polyamine biosynthesis. *Eukaryotic Cell*, 8(5):747–755, 2009.
- [24] Erin K. Willert and Margaret A. Phillips. Regulated expression of an essential allosteric activator of polyamine biosynthesis in African Trypanosomes. *PLoS Pathogens*, 4:1–12, 2008.
- [25] Alan J. Bitonti, Timothy L. Byers, Tammy L. Bush, Patrick J. Casara, Cyrus J. Bacchi, JR. Allen B. Clarkson, Peter P. McCann, and Albert Sjoerdsma. Cure of *trypanosoma brucei brucei* and *trypanosoma brucei rhodesiense* infections in mice with an irreversible inhibitor of S-Adenosylmethione decarboxylase. *Antimicrobial agents and chemotherapy*, 34(8):1485–1490, 1990.
- [26] Mark R. Ariyanayagam, Sandra L. Oza, Maria Lucia S. Guther, and Alan H. Fairlamb. Phenotypic analysis of trypanothione synthetase knockdown in the African trypanosom. *Journal of Biochemistry*, 391:425–432, 2005.
- [27] Torsten Söderström and Petre Stoica. *System Identification*. Prentice Hall, 1989.
- [28] Lennart Ljung. Perspective on system identification. Plenary Session, 17th IFAC World Congress, Seoul, Korea, 2008.
- [29] Erin K. Willert, Richard Fitzpatrick, and Margaret A. Phillips. Allosteric regulation of an essential trypanosome polyamine biosynthetic enzyme by a catalytically dead homolog. *PNAS*, 104(20):8275–8280, 2007.
- [30] Tracy Clyne Beswick, Erin K. Willert, and Margaret A. Phillips. Mechanisms of allosteric regulation of *trypanosoma cruzi* S-Adenosylmethionine decarboxylase. *Biochemistry*, 45:7797–7807, 2006.
- [31] Lutz Birnbaumer, Cynthia F. Bearer, and Ravi Iyengar. A two-state model of an enzyme with an allosteric regulatory site capable of metabolizing the regulatory ligand. *The Journal of Biological Chemistry*, 255(8):3552–3557, 1980.
- [32] Alan J. Bitonti, Jennifer A. Dumont, and Peter P. McCann. Characterization of *trypanosoma brucei brucei* S-adenosyl-L-methione decarboxylase and its inhibition by Berenil, pentamidine and methylglyoxal bis(guanylhydrazone). *The Journal of Biological Chemistry*, 237:685–689, 1986.
- [33] Anthony E. Pegg and Gregg Jacobs. Comparison of inhibitors of S-adenosylmethionine decarboxylase from different species. *Biochemistry*, 213:495–502, 1983.
- [34] N. Yarlett, J. Garofalo, B. Goldberg, M. A. Ciminelli, V. Ruggiero, J. R. Sufrin, and C. J. Bacchi. S-adenosylmethionine synthetase in bloodstream *Trypanosoma brucei*. *Biochim Biophys Acta*, 24(1):68–76, 1993.
- [35] Laurence Christa, Joelle Kersual, Joelle Auge, and Jean-Louis Perignon. Methylthioadenosine toxicity and metabolism to methionine in mammalian cells. *Journal of Biochemistry*, 255:145–152, 1988.
- [36] Jr. Peter S. Backlund, Changtung P. Chang, and Roberts A. Smith. Identification of 2-Keto-4-methylthiobutyrate as an intermediate compound in methionine synthesis from 5'-Methylthioadenosine. *The Journal of Biological Chemistry*, 257(8):4196–4202, 1982.
- [37] Alan J. Bitonti, Susan E. Kelly, and Peter P. McCann. Characterization of spermidine synthase from *trypanosoma brucei brucei*. *Molecular and Biochemical Parasitology*, 13:21–28, 1984.
- [38] Janice R. Sufrin, Arthur J. Spiess, Jr. Canio J. Marasco, Donna Rattendi, and Cyrus J. Bacchi. Novel trypanocidal analogs of 5'-(methylthio)-adenosine. *Antimicrobial Agents and Chemotherapy*, 52(1):211–219, 2008.
- [39] Bradley J. Berger, Wei Wei Dai, Hsin Wang, Ruth E. Stark, and Anthony Cerami. Aromatic amino acid transamination and methionine recycling in trypanosomatids. *Proc. Natl. Acad. Sci.*, 93:4126–4130, 1996.
- [40] Janice R. Sufrin, Steven R. Meshnick, Arthur J. Spiess, Joanne Garofalo-Hannan, Xing-Qing Pan, and Cyrus J. Bacchi. Methionine recycling pathways and antimalarial drug design. *Antimicrobial Agents and Chemotherapy*, 39(11):2511–1515, 1995.
- [41] M. K. Riscoe, A. J. Ferro, and H. Fitchen. Methionine recycling as a target for antiprotozoal drug development. *Parasitology Today*, 5(10):330–333, 1989.
- [42] C. W. Porter and J. R. Sufrin. Interference with polyamine biosynthesis and/or function by analogs of polyamines or methionine as a potential anticancer chemotherapeutic strategy. *Anticancer Res.*, 6(4):525–542, 1986.
- [43] Rosa M. Reguera, Carmen M. Redondo, Yolanda Perez-Pertejo, and Rafael Balana-Fouce. S-adenosylmethionine in protozoan parasites: Functions, synthesis and regulation. *Molecular & Biochemical Parasitology*, 152:1–10, 2007.
- [44] L. Y. Ghoda, T. M. Savarese, C. H. Northrup, Jr. R. E. Parks, J. Garofalo, L. Katz, B. B. Ellenbogen, and C. J. Bacchi. Substrate specificities of 5'-deoxy-5'-methylthioadenosine phosphorylase from *Trypanosoma brucei brucei* and mammalian cells. *Mol. Biochem. Parasitol.*, 27:109–118, 1988.

- [45] Cyrus J. Bacchi, Janice R. Sufrin, Henry C. Nathan, Arthur J. Spoess, Thomas Hannan, Joanne Garofalo, Karen Alecia, Lillian Katz, and Nigel Yarlett. 5'-Alkyl-substituted analogs of 5'-Methylthioadenosine as Trypanocides. *Antimicrobial Agents and Chemotherapy*, 35(7):1315–1320, 1991.
- [46] N. Yarlett, A. Quamina, and C. J. Bacchi. Protein methylase in *Trypanosoma brucei brucei*: activities and response to DL-alpha-difluoromethylornithine. *Journal of General Microbiology*, 137(3):717–724, 1991.
- [47] Michael Duszenko, Michael A. J. Ferguson, Gretel S. Lamont, Mary R. Rifkin, and George A. M. Cross. Cysteine eliminates the feeder cell requirement for cultivation of *trypanosoma brucei*. *The Journal of Experimental Medicine*, 162:1256–1263, 1985.
- [48] Jens Martens-Lobenhoffer, Sylvia Postel, Uwe Troger, and Stefanie M. Bode-Boger. Determination of ornithine in human plasma by hydrophilic interaction chromatography-tandem mass spectrometry. *Journal of Chromatography*, 855:271–275, 2007.
- [49] Xu Gu. *Systems Biology Approaches to the Computational Modelling of Trypanothione Metabolism in Bloodstream-form Trypanosoma brucei*. Dissertation, The University of Glasgow, Glasgow, UK, 2010.
- [50] Omri Erez, Dan Goldstaub, Joseph Friedman, and Chaim Kahana. Putrescine activates oxidative stress dependent apoptotic death in ornithine decarboxylase overproducing mouse myeloma cells. *Experimental Cell Research*, 281:148–156, 2002.
- [51] Toshikazu Suzuki, Yong He, Keiko Kashiwagi, Yasuko Murakami, Shin-Ichi Hayashi, and Kazuei Igarashi. Antizyme protects against abnormal accumulation of toxicity of polyamines in ornithine decarboxylase-overproducing cells. *PNAS*, 91:8930–8934, 1994.
- [52] Viridiana Olin-Sandoval, Zabdi González-Chávez, Miriam Berzunza-Cruz, Ignacio Martínez, Ricardo Jasso-Chávez, Ingeborg Becker, Bertha Espinoza, Rafael Moreno-Sánchez, , and Emma Saavedra. Drug target validation of the trypanothione pathway enzymes through metabolic modelling. *FEBS Journal*, pages 1811–1833, 2012.
- [53] BARBARA M. BAKKER, R. LUISE KRAUTH-SIEGEL, CHRISTINE CLAYTON, KEITH MATTHEWS, MARK GIROLAMI, HANS V. WESTERHOFF, PAUL A. M. MICHELS, RAINER BREITLING, and MICHAEL P. BARRETT. The silicon trypanosome. *Parasitology*, 137:1333–1341, 2010.

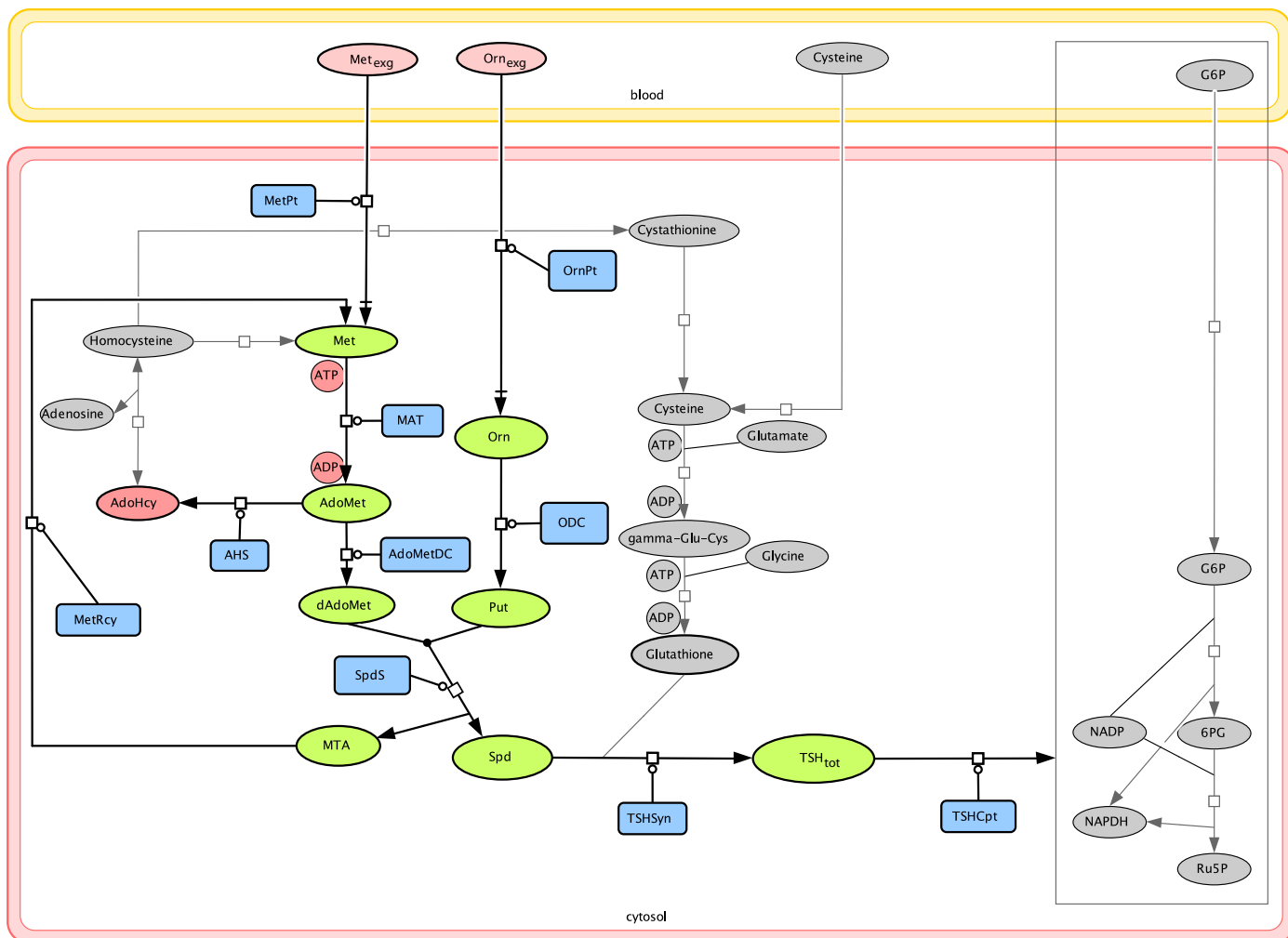
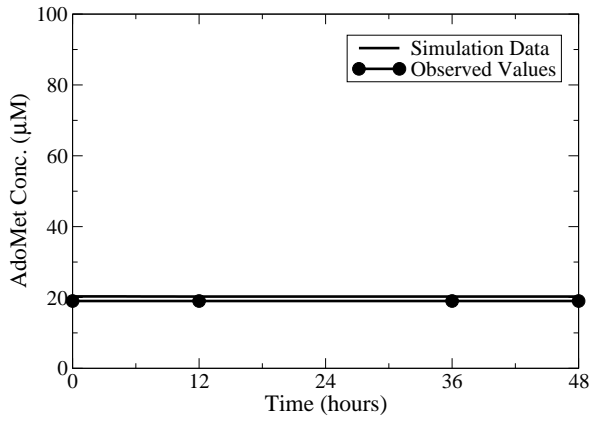
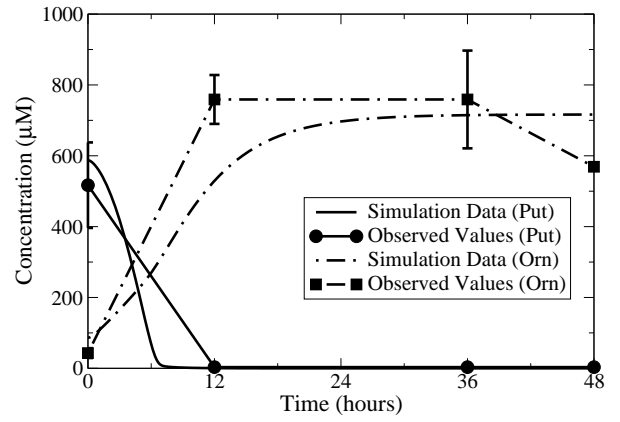


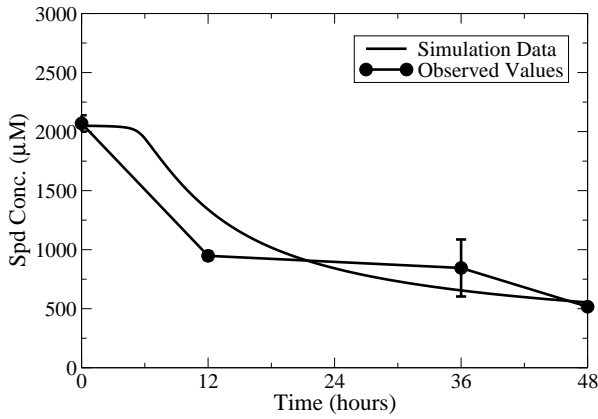
Figure 1: **A detailed graphical representation of trypanothione metabolism.** Ovals in the blood compartment represent constant exogenous metabolites to be assimilated into the cytosolic compartment. Ovals in the cytosolic compartment represent intra-cellular metabolites that are time-dependent variables. Edges represent chemical conversions between model components with arrows indicating reaction directionality. Metabolites and reactions constituting the polyamine biosynthetic pathway that are considered in this model are highlighted in bold, with time-variant metabolites shown in green and constant metabolites shown in pink. Enzymes catalysing each active elementary step in the pathway are denoted with blue boxes. The remaining modules of the network shown in grey are not modelled but help gaining an overall picture of the metabolism. Abbreviations of polyamine metabolites: Met, methionine; AdoMet, S-adenosylmethionine; dAdoMet, decarboxylated AdoMet; MTA, methylthioadenosine; AdoHcy, S-adenosylhomocysteine; Orn, ornithine; Put, putrescine; Spd, spermidine; TSH_{tot} , total trypanothione; Met_{exg} , exogenous methionine; Orn_{exg} , exogenous ornithine; . Abbreviations of intra-cellular polyamine enzymes: MetPt, Met uptake enzyme; MAT, AdoMet synthase; AHS, methyltransferase; AdoMetDC, AdoMet decarboxylase; MetRcy, Met recycling enzyme; OrnPt, Orn uptake enzyme; ODC, Orn decarboxylase; SpdS, Spd synthase; TSHSyn, TSH_{tot} synthesis catalyst; TSHCpt, TSH_{tot} consumption catalyst.



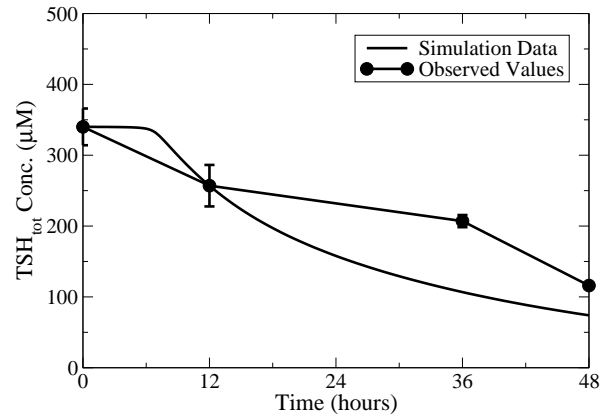
(a) AdoMet



(b) Orn,Put

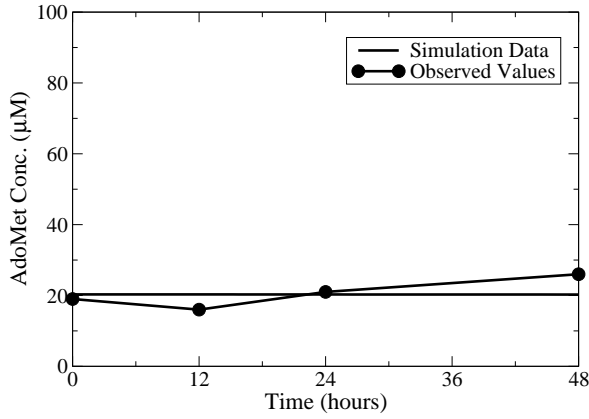


(c) Spd

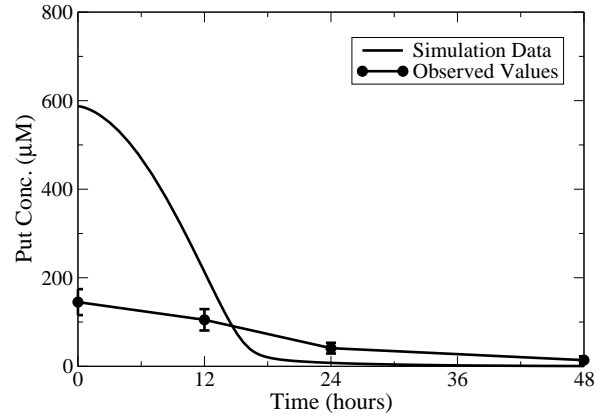


(d) TSH_{tot}

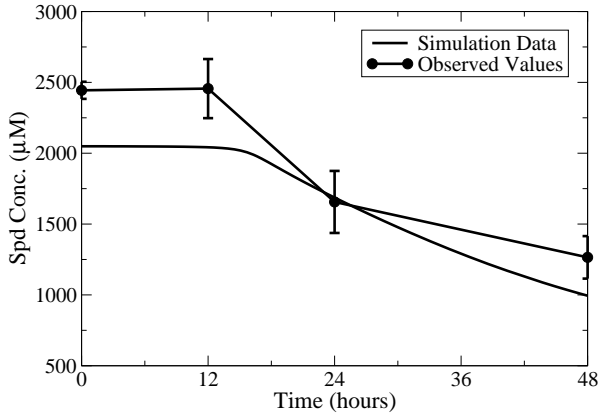
Figure 2: Model predictions on polyamine dynamics under DFMO treatment compared with experimental data provided by Fairlamb et al. [10]. Enzyme activity of ODC was modelled as a time-dependent variable. AdoMet contents are measured by Xiao et al. [23].



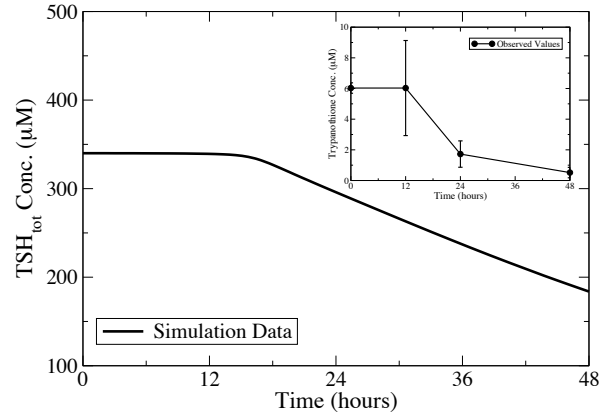
(a) AdoMet



(b) Put

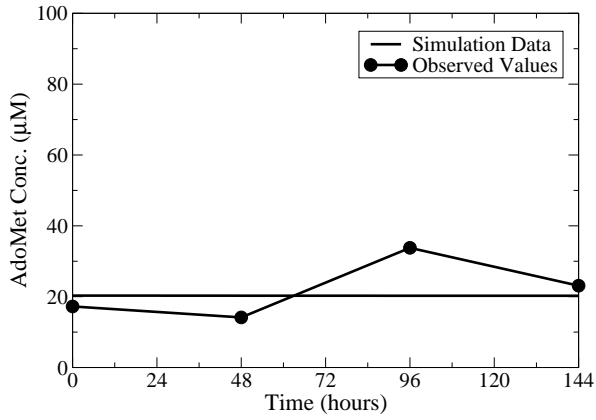


(c) Spd

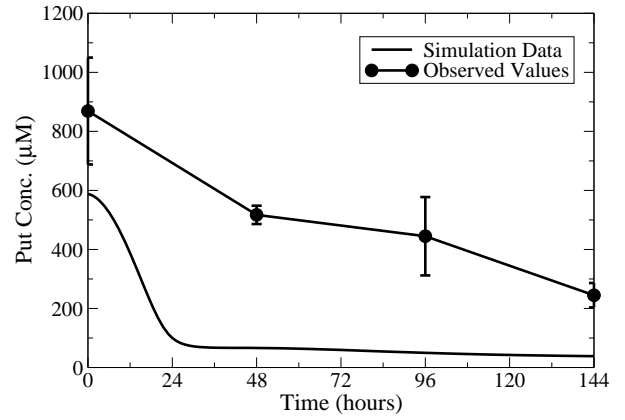


(d) TSH_{tot}

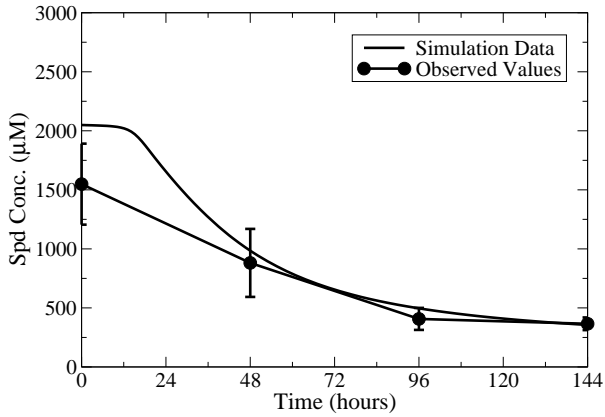
Figure 3: Time-series simulation of the effect of ODC inhibition on polyamine levels (lines without symbols) compared with observed values *in vitro* (lines with symbols). Enzyme specificity of ODC was modelled as a time-dependent variable during the simulation with λ_E equal to 0.0016. AdoMet dynamics observed by Xiao et al. [23] were adopted as experimental data.



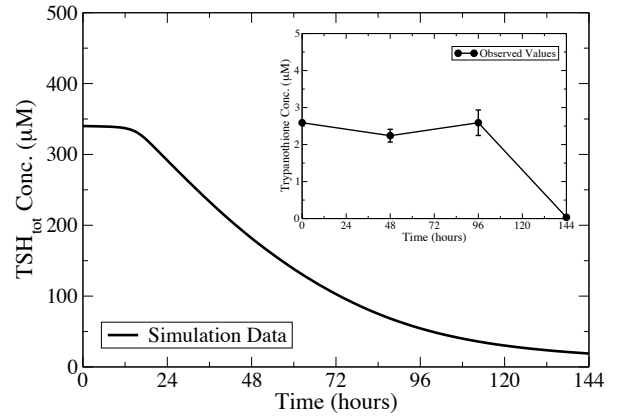
(a) AdoMet



(b) Put

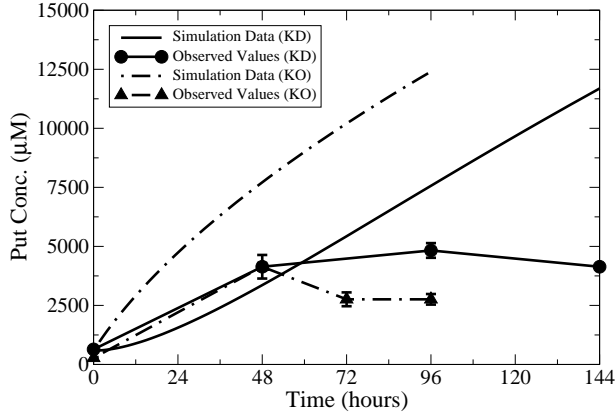


(c) Spd

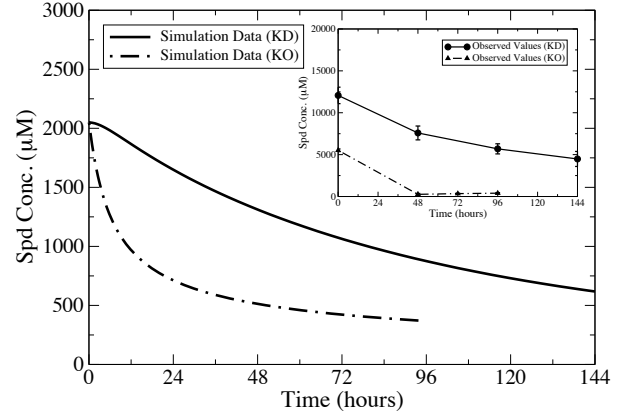


(d) TSH_{tot}

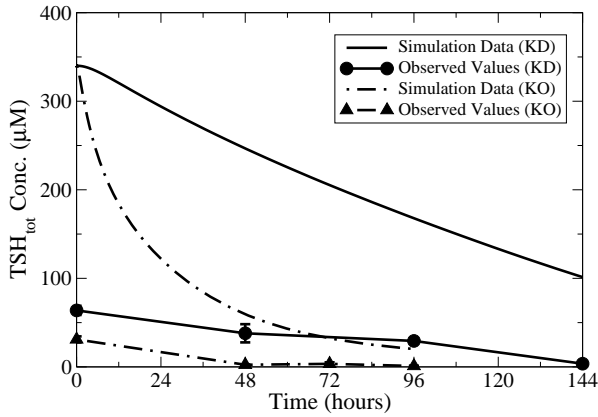
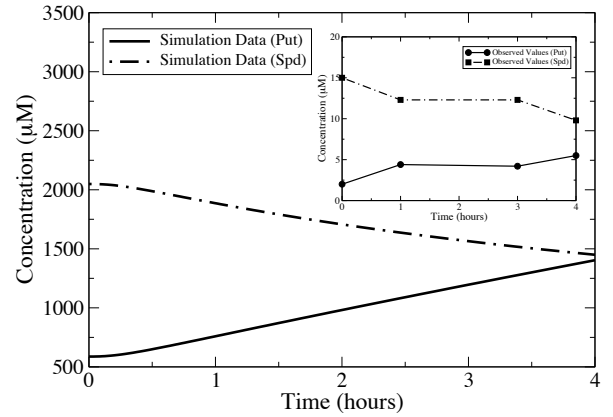
Figure 4: Time-series simulation of SpdS knockdown on polyamine levels (lines without symbols) compared with observed values *in vivo* (lines with symbols). Enzyme specificity of SpdS was modelled as a time-dependent variable with λ_E equal to 0.0016. Observed values made by Xiao et al. [23] are used in the figure.



(a) Put



(b) Spd

(c) TSH_{tot} 

(d) MDL-mediated Induction

Figure 5: **Effects of AdoMetDC knockdown (KD) and prozyme knockout (KO) on polyamine levels in time-dependent simulations (a-c).** In KD simulations, total AdoMetDC concentration ($[AdoMetDC^T]$) was modelled as a time-dependent variable with λ_E equal to 0.0004 to represent the 70% activity down-regulation within 2 days of induction. In KO simulations, the factor $1 - \beta$ representing the percent of the complex AdoMetDC|prozyme taking up the total enzyme AdoMetDC is set to zero to represent full prozyme removal. Observed values made by Willert et al. [24] are used in the figure. In (d), Put and Spd dynamics in response to a 98% knockdown of AdoMetDC concentration by interacting with the MDL component are compared with the experimental observations from [25]. During the simulation, total enzyme concentration of AdoMetDC was modelled using an exponential decay function with λ_E set to 0.07 to mimic a 98% knockdown within 1 hour of induction.

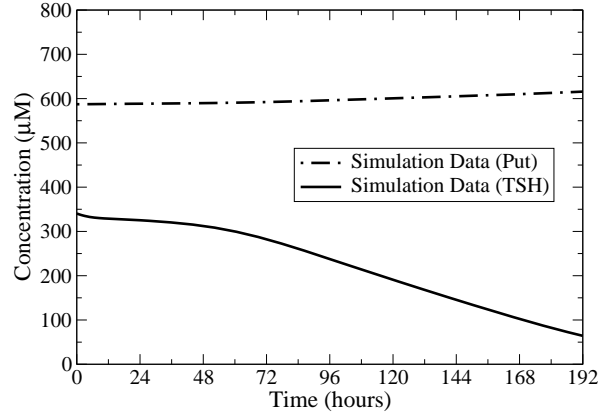


Figure 6: TSH_{tot} dynamics over 8 days of TSHSyn RNAi induction. During the simulation, TSHSyn activity (V_{max}^{TSHSyn}) was modelled as a time-dependent variable using the exponential decay function with λ_E set to 0.00045.

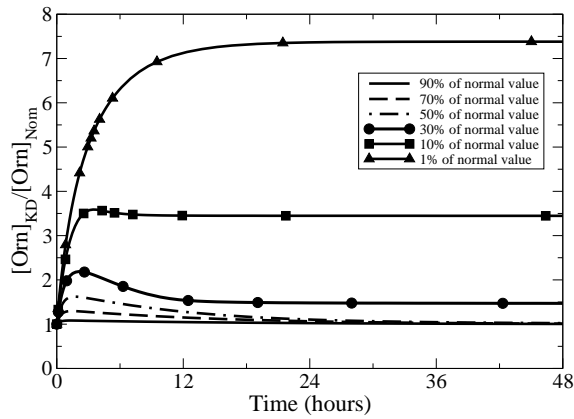
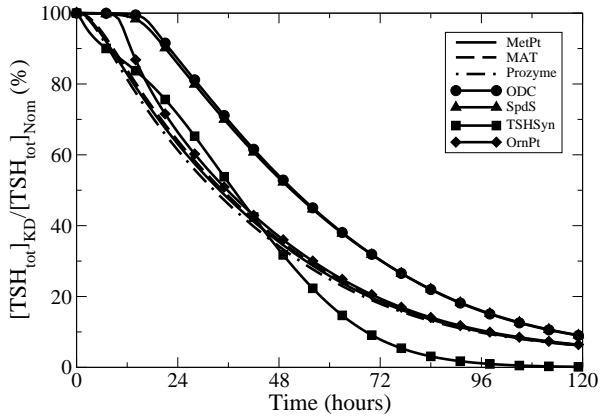
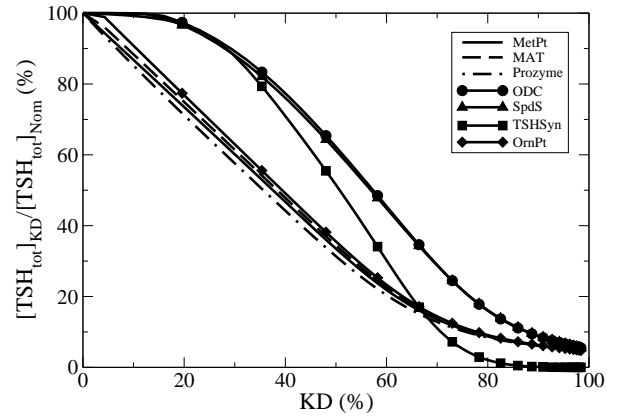


Figure 7: Orn dynamics over 2 days after ODC activity depression. During the simulation, ODC activity (V_{max}^{ODC}) was modelled as a time-independent constant by multiplying the normal value by the percentage amount.

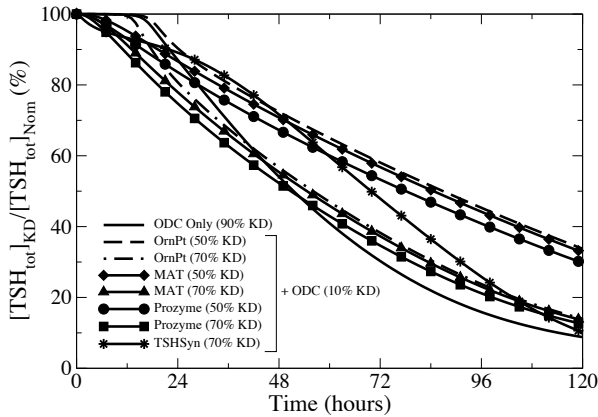


(a) Key Enzymes (90% KD)

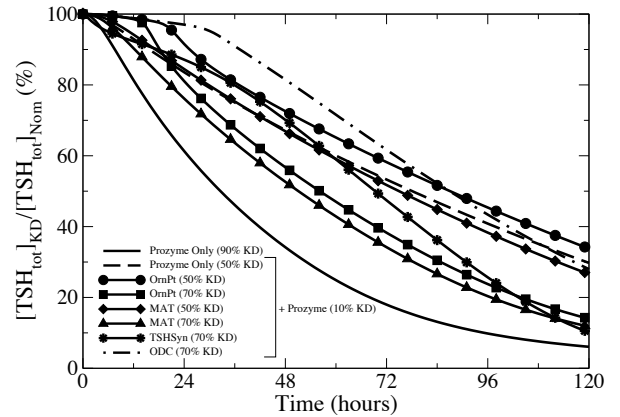


(b) Key Enzymes (KD %)

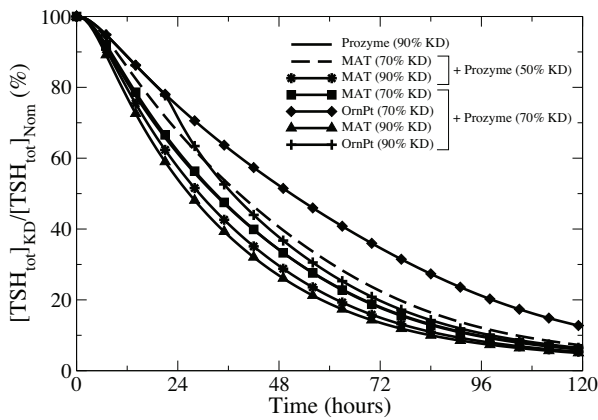
Figure 8: **Studies of changes in TSH_{tot} concentration under different perturbations.** In (a) time-series TSH_{tot} concentration values are calculated over a simulated time span of 5 days subject to a 90% decrease of individual enzyme activity. A 90% knockdown of AdoMetDC enzyme concentration and a 90% prozyme knockdown were found to follow a similar pattern of TSH_{tot} dynamics, and only prozyme inhibition is shown. In (b) TSH_{tot} concentration values at the end of the simulated time span (5 days) are calculated subject to various degrees of knockdown (KD) for individual enzymes. In both figures, the percentage of TSH_{tot} concentration under perturbed ($[TSH_{tot}]_{KD}$) and normal ($[TSH_{tot}]_{Nom}$) conditions is plotted. In all cases, enzyme activities (V_{max}^E) are time-dependent variables subject to specific inhibition within 24 hours of simulation.



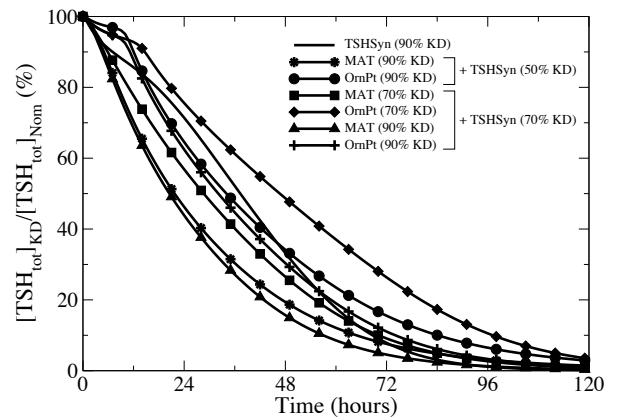
(a) ODC



(b) Prozyme



(c) Prozyme (more)



(d) TSHSyn

Figure 9: **Studies of combination chemotherapeutic regimens.** Percentage of TSH_{tot} concentration under perturbed ($[TSH_{tot}]_{KD}$, over a simulated time span of 5 days) and normal ($[TSH_{tot}]_{Nom}$) conditions. In individual model simulations (a) and (b), a 10% enzyme knockdown (KD) of ODC and prozyme is applied in conjunction with down-regulation of other key pathway enzymes and the simulation results from individual and combined perturbations are compared. In (c) and (d), the inhibitory effects on TSH_{tot} were examined for combinations of medium to strong depression of prozyme and TSHSyn and different levels of knockdowns of other enzymes. In all cases, enzyme activities (V_{max}^E) are time-dependent variables subject to specific inhibition within 24 hours.